Journal of Alloys and Compounds 584 (2014) 590–599

Contents lists available at ScienceDirect

Journal of Alloys and Compounds

journal homepage: www.elsevier.com/locate/jalcom

Melt processed single phase hollandite waste forms for nuclear waste immobilization: $Ba_{1.0}Cs_{0.3}A_{2.3}Ti_{5.7}O_{16}$; A = Cr, Fe, Al

Jake Amoroso [a], James Marra [a], Steven D. Conradson [b], Ming Tang [b], Kyle Brinkman [a,*]

[a] Savannah River National Laboratory, Aiken, SC 29808, USA
[b] Los Alamos National Laboratory, Los Alamos, NM 87545, USA

ARTICLE INFO

Article history:
Received 20 August 2013
Received in revised form 6 September 2013
Accepted 12 September 2013
Available online 21 September 2013

Keywords:
Waste form
Nuclear materials
Chemical durability

ABSTRACT

Cs is one of the more problematic fission product radionuclides to immobilize due to its high volatility at elevated temperatures, ability to form water soluble compounds, and its mobility in many host materials. The hollandite structure is a promising crystalline host for Cs immobilization and has been traditionally fabricated by solid state sintering methods. This study presents the structure and performance of $Ba_{1.0}Cs_{0.3}A_{2.3}Ti_{5.7}O_{16}$; A = Cr, Fe, Al hollandite fabricated by melt processing. Melt processing is considered advantageous given that melters are currently in use for High Level Waste (HLW) vitrification in several countries. This work details the impact of Cr additions that were demonstrated to (i) promote the formation of a Cs containing hollandite phase and (ii) maintain the stability of the hollandite phase in reducing conditions anticipated for multiphase waste form processing.

1. Introduction

Waste treatment technologies are an integral component to the United States' advanced nuclear fuel cycle program. Successful waste treatment and storage are necessary to support next-generation nuclear energy development. The United States Department of Energy (DOE) under the Fuel Cycle Research and Development (FCR&D) program is developing fuel reprocessing technology that would separate the fuel into several fractions, thus, partitioning the waste into groups with common chemistry. A single waste form that can host all the waste elements in the projected advanced nuclear fuel cycles – to include a Cs/Sr separated waste stream, the Trivalent Actinide – Lanthanide Separation by Phosphorous reagent Extraction from Aqueous Komplexes (TALSPEAK) waste stream, the transition metal fission product waste stream resulting from the transuranic extraction (TRUEX) process, MoO_3, and noble metals (CsSr–Ln–TM) – is most desirable [1].

The traditional method for waste encapsulation is to use borosilicate glass, a practice currently used to handle both defense and commercial waste [2]. However, the low solubility of transition metals, including Mo in the glass present challenges to achieving desirable and attainable waste loadings using immobilization in borosilicate glass [3]. Recent work has focused on fully crystalline and glass/ceramic composites to address these concerns and develop the next generation of waste immobilization materials [4,5]. Ceramic (or crystalline) waste forms incorporate radionuclides in the waste as part of their crystal structure and therefore appropriate engineered materials can accommodate diverse waste. Tailoring a ceramic waste form is based on the knowledge that there are many naturally produced minerals containing radioactive and non-radioactive species very similar to the radionuclides of concern in wastes from fuel reprocessing. Durable ceramic waste forms that incorporate a wide range of radionuclides have the potential to broaden the available disposal options and to lower the storage and disposal costs associated with advanced fuel cycles.

Multiphase ceramics targeting an assemblage of titanate phases have been successfully demonstrated to incorporate various radioactive waste elements into a number of crystalline phases. Most notable are the SYNROC – and its derivatives – materials developed in the 80s that have been primarily produced with solid-state sintering methods [6,7]. In these materials, Cs is incorporated into a hollandite phase however; the high volatility of Cs and the tendency for Cs_2O to react with other oxides have required the use of hot-pressing in the presence of reducing agents to ensure the avoidance of non-durable phases [8]. Melt processing of waste forms is advantageous since melters are already in use for High Level Waste (HLW) vitrification in several countries, and melter technology greatly reduces the potential for airborne contamination as compared to processes involving extensive powder handling operations. Melt processing of select single phase ceramics including zirconolite as well as actinide containing multiphase ceramics based on muratite have been recently demonstrated using cold crucible induction melting technology (CCIM) [9,10]. However, to date melt processed SYNROC from waste streams of interest to the U.S. FCR&D program have not been demonstrated via CCIM

* Corresponding author. Tel.: +1 803 725 9843.
E-mail address: kyle.brinkman@srnl.doe.gov (K. Brinkman).

0925-8388/$ - see front matter © 2013 Elsevier B.V. All rights reserved.
http://dx.doi.org/10.1016/j.jallcom.2013.09.087

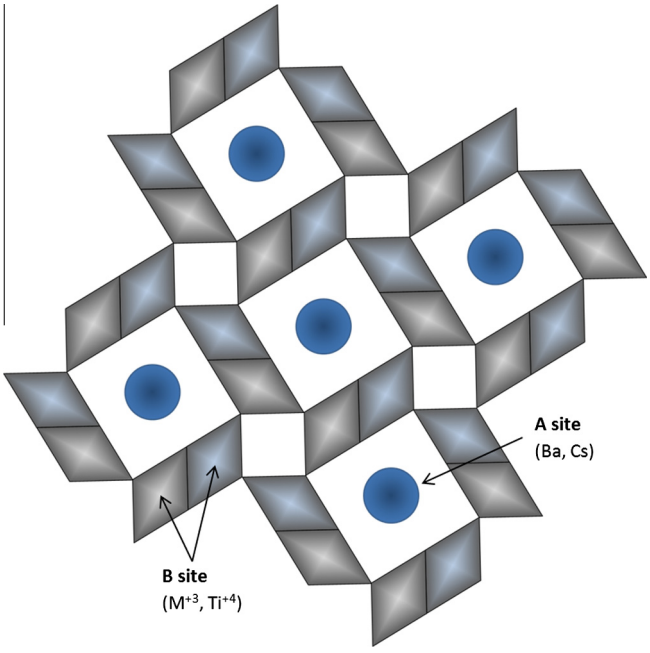

Fig. 1. Idealized two-dimensional [001] projection of the tetragonal hollandite structure showing octahedra pairs lining the tunnels and A site cation positions.

primarily due to issues related to Cs–Mo formation and the limited understanding of fully crystalline phase formation derived from high temperature melts. The goal of this work is to demonstrate the feasibility of melt processing technologies to produce Cs containing single phase hollandite ceramic waste forms. Hollandite compositions and processing conditions were developed to incorporate Cs into the crystalline matrix under reducing conditions where Cs–Mo formation is unfavorable. The resulting phases and processes will be incorporated into future work on melt processing of multi-phase crystalline waste forms from combined CsSr–Ln–TM waste streams.

Cs is one of the more problematic fission product radionuclides to immobilize due to its high volatility at elevated temperatures, ability to form water soluble compounds, and its mobility in many host materials. Hollandite-type structures appear to be a good candidate for Cs immobilization compared to silicate or phosphate ceramics which are difficult to fabricate as single phases with high densities, or to nuclear glasses in which the alkaline elements are the most mobile waste species in aqueous environments. There are natural analogues of hollandite including ankagite, found in dolomitic marble in the Apuan Alps in Tuscany, Italy which demonstrate the long term stability of these crystal structures over geologic timescales of interest for nuclear waste immobilization [11]. The hollandite group of minerals has the formula $A_xB_yC_{8-y}O_{16}$ where the B and C cations are surrounded by octahedral configuration of oxygen [12]. In the hollandite structure, columns of four pairs of edge sharing octahedra connected to each other on the corners form tunnels running parallel to the short crystal axis. The tunnel cross-section is generally square, but will distort as a rhombus depending on the particular hollandite symmetry which can be either monoclinic (rhombus) or tetragonal (square) depending on the radius ratio of the A–B site cations. Fig. 1 depicts a two-dimensional schematic of the tetragonal hollandite structure. In hollandite structures used for nuclear waste incorporation, the A site is occupied by Cs/Rb and Ba, the B site by Al^{3+} and Ti^{+3}, and the C site by Ti^{+4} resulting in the general formula of $(Ba_xCs_y)(Ti, Al)^{+3}_{2x+y}(Ti^{+4}_{8-2x-y})O_{16}$ [13].

2. Composition development

Solution processing and bulk oxide routes have been used to fabricate single phase $(Ba_xCs_y)(Al_{2x+y}Ti_{8-2x-y}O_{16})$ hollandite. Under oxidizing conditions, $(Ba_xCs_y)(Al_{2x+y}Ti_{8-2x-y}O_{16})$ ceramics prepared through such methods often resulted in multiphase assemblages when heated nominally at 1200 °C even for extended periods of time (>96 h) and exhibited poor Cs leaching behavior in water [14]. The poor Cs leaching in hollandites prepared by either method has been attributed to secondary phases that are metastable and easily leached such as $CsAlTiO_4$. Kesson and Roth demonstrated that replacing a portion of the Al^{3+} with Ti^{3+} suppressed secondary phase formation and decreased Cs leach rates by an order of magnitude [8]. Moreover, Kesson demonstrated that metal powder (Ti) additions to the batch material or hot pressing in graphite were effective methods for controlling the redox conditions during sintering [8].

Although it is difficult to form a $(Ba_xCs_y)(Ti, Al)^{+3}_{2x+y}(Ti^{+4}_{8-2x-y})O_{16}$ single phase hollandite in oxidizing atmospheres, other M^{+3} elements such as Fe^{3+} can be substituted into the $(Ba_xCs_y)(Ti, Al)^{+3}_{2x+y}(Ti^{+4}_{8-2x-y})O_{16}$ phase targeting $Ba_{1.0}Cs_{0.28}Al_{1.46}Fe_{0.82}Ti_{5.72}O_{16}$ which has been shown to form a stable single phase incorporating Cs. Recently, single phase hollandite materials containing mixtures of divalent and trivalent cations have been fabricated by solution mixtures and oxide routes based on the general formula $(Ba_xCs_y)(M^{+3}_zTi^{+4}_{8-z})O_{16}$ with M = Mn^{+3}, Fe^{+3}, Ga^{+3}, Cr^{+3}, Sc^{+3}, Ti^{+3}, Ni^{+2}, Co^{+2}, Zn^{+2}, and Mg^{+2} where $z = 2x + y$ for trivalent cations and $z = x + y/2$ for divalent cations for charge compensation [14–16]. In general, many of those trivalent and divalent cations were effective in promoting Cs incorporation into the hollandite, but also promoted secondary phase formation. Ga produced a phase similar to $CsAlTiO_4$, which is assumed to be non-durable. Sc and Mg additions resulted in a mixture of hollandite and secondary phases and did not readily react to changes in processing. Ni, Co, Zn, and Mn exhibited secondary phases, but are generally not considered to be durability limiting. Several groups have found that Cr doped samples resulted in single phase formation; Carter was able to fully substitute Cs for Ba in Cr analogue and Aubin-Chevaldonnet et al. showed Cr samples were not fully dense at intermediate sintering temperatures (1200 °C) with the resulting structures demonstrating ~50% of Cs retention [14]. All of these groups suggested that Al/Fe additions were a good choice because they enhanced single phase formation and exhibited high Cs incorporation. However, while these additives may be sufficient for single phase hollandite formation, recent work at Savannah River National Laboratory (SRNL) showed that in air, Cs partitioned to non-durable Mo and Ti phases when a Al/Fe hollandite was incorporated into a multiphase ceramic composition [4].

Despite the large body of work on the topic, the literature is not consistent. This is particularly apparent when different preparation routes (sol–gel versus solid state methods) and densification techniques (Hot Isotactic Pressing versus conventional press and sintering) were used. The approach used in this work was to select an additive (or combination of additives) to overcome the limitations associated with the hollandite phase as it relates to inclusion in a multiphase waste form processed by a melt and crystallization process. In particular, the hollandite phase should readily and preferentially incorporate Cs, be robust to wide compositional changes, chemically durable, and less sensitive (compared to $Ba_xCs_yAl_{2x+y}Ti_{8-2x-y}O_{16}$) to redox conditions. In addition, a combined waste stream is anticipated to contain MoO_3 which is known to preferentially react with Cs_2O and it is recognized that reducing atmospheres are a proven method to suppress Cs–Mo secondary phase formation. The approach in this work was to first identify

an additive that promoted single phase hollandite formation and Cs incorporation across a wide range of redox conditions resulting in a flexible Cs immobilization host material.

Dopants which have an atomic radius appropriate for the M^{+3} site in the hollandite to facilitate Cs incorporation (Fe^{+3} coexisting with Al^{+3} in the B site) are not found in the anticipated waste streams. However, taking into consideration the corrosion products and other additives from the separations processes, appreciable concentrations of Cr_2O_3 and/or Fe_2O_3 (~1–10 wt.%) arising from Purex or JW-A processing contamination can be expected [17,18].

Cr was identified as a potential additive because it has consistently compelled single phase hollandite formation in air throughout the literature and there is little data published concerning the pure Cr analogue, particularly for melt processed samples in varying redox conditions.

3. Experimental

In this work, three nominal hollandite compositions, $Ba_{1.0}Cs_{0.3}Cr_{2.3}Ti_{5.7}O_{16}$ – referred to as Cr–Hol, $Ba_{1.0}Cs_{0.3}Cr_{1.0}Al_{0.3}Fe_{1.0}Ti_{5.7}O_{16}$ – referred to as CAF–Hol, and $Ba_{1.0}Cs_{0.3}Fe_{2.3}Ti_{5.7}O_{16}$ – referred to as Fe–Hol were prepared and characterized in terms of phase formation, elemental partitioning, and durability to aqueous corrosion. Although Al–Fe containing hollandite has been widely studied the Cr–Al–Fe composition was developed to exploit the Cr ionic radius that is less than Fe^{3+} but greater than Al^{3+} which could be expected to promote single phase formation while maximizing Cs incorporation. The pure Fe analogue, expected to be multiphase and exhibit poor durability, was included as a baseline to compare results. It is anticipated that in future studies, optimized hollandite compositions will be incorporated into multiphase waste forms processed in reducing environments in order to reduce Cs–Mo association. Based on that expectation, a variety of reducing conditions were evaluated including the use of solid state reducing agents (Ti/TiO_2) and reducing gas environments ($1\%H_2/Ar$).

3.1. Fabrication and melt processing

3.1.1. Batch preparation

Stoichiometric amounts of reagent-grade oxide and carbonate powders (99.5% purity) were combined in a 500 ml plastic bottle with zirconia milling media, filled 2/3 full with deionized water, and agitated in a tumbler mixer for 1 h. Subsequently, each slurry was poured into a separate pan along with additional rinse water used to collect any batch material remaining on the milling media and bottles. Each pan was transferred to an oven where the slurry was dried for several days at 90 °C. The dried material was bagged and used as feed stock for synthesis experiments.

3.1.2. Melt processing

Approximately 20 g samples feed stock was placed loosely into a covered alumina crucible. The samples were heated in air and in 1% H_2 (99% Ar) reducing atmosphere. Ti metal and TiO_2 additions were made to some batches prior to synthesis. For those samples, prepared mixtures of 2.0 wt.% Ti metal and 7.0 wt.% TiO_2 were manually mixed into each batch. Samples were heated at approximately 15 K/min, held at 1500 °C for 20 min, and furnace cooled (powered off furnace). Table 1 summarizes the experimental matrix including hollandite composition, solid state sintering additives and processing conditions used in this work.

3.2. Characterization

3.2.1. Phase identification and microstructure

Samples were characterized with X-ray diffraction (XRD, D8 Advance, Bruker AXS Inc., Madison, WI) to identify the resulting phase(s). Portions of each sample were initially ground in an automatic Spex mill for 4 min. Subsequently, the powders were hand ground in agate with alcohol and mounted to a glass slide using a collidion/Amyl Acetate solution. The measurement conditions scanned 5–70° 2θ.

Scanning Electron Microscopy (SEM) and Energy-Dispersive X-ray Spectroscopy (EDS) measurements were performed at SRNL with a Hitachi TM3000 SEM and at the Electron Microscopy Lab (EML) at LANL with a FEI Inspect SEM. Samples were coated with 2 nm of carbon to prevent surface charging. A powder sample was prepared for transmission electron microscopy (TEM) examination. The microstructure information was characterized by a TEM (Fei Tecnai F30) with a point-to-point resolution of 0.21 nm operating at 300 kV.

3.2.2. Chemical composition

Inductively Coupled Plasma–Atomic Emission Spectroscopy (ICP–AES) was used to measure Ba, Cr, Fe, Al, and Ti concentrations and Inductively Coupled Plasma–Mass Spectroscopy (ICP–MS) was used to measure Cs concentrations as Cs cannot be measured by ICP–AES. A representative amount from each sample was prepared via a sodium peroxide fusion (PF) method for cation measurements – typical lithium–metaborate fusion (LM) was not sufficient to dissolve the high concentrations of TiO_2 and Cr_2O_3. Each sample was prepared in duplicate. Prepared samples were analyzed twice for each element of interest by ICP, with the instrumentation being re-calibrated between the duplicate analyses. Glass standards were also intermittently measured to ensure the performance of the ICP–AES instrument over the course of the analyses. The measured cation concentrations were converted to their respective oxide to obtain a wt.% of each component oxide.

3.2.3. Oxidation states

The Fe^{2+}/Fe^{3+} and Fe^{2+}/Fe (total) ratios were determined from an absorption method using a UV–Vis spectrometer. Samples were dissolved in a sulfuric–hydrofluoric acid mixture, containing ammonium vanadate to preserve the Fe^{2+} content. Boric acid was added to destroy iron–fluoride complexes and ferrozine was added to form ferrous–ferrozine complexes for the determination of Fe^{2+} content. An additional measurement with ascorbic acid addition to reduce Fe^{3+}–Fe^{2+} with a second absorbance measurement was used to determine total Fe [19].

X-ray Absorption Spectroscopy (XAS), including both Extended X-ray Absorption Fine Structure (EXAFS) and X-ray Absorption Near Edge Structure (XANES) measurements were performed on end stations 4–2 and 11–2 of the Stanford Synchrotron Radiation Laboratory, under dedicated synchrotron X-ray production conditions (3.0 GeV e, 45–100 mA). Fe and Cr K XAFS spectra were measured on beamline 11–2 at the Stanford Synchrotron Radiation Lightsource with a 3.0 GeV beam energy and 500 mA stored current in the fluorescence mode using a 100 element monolithic Ge detector and X-ray Instrumentation Associates digital amplifiers. Total count rates in each element were kept below 50–60 kHz. The spectra were calibrated by assigning the first inflection point of a Fe foil to 7111.3 eV. The ionization energies used for calculation of the photoelectron wave vector magnitude were 6009 and 7118 eV for, respectively, Cr and Fe. The spectra were normalized by offsetting them so that the energy of a second order polynomial fit through the pre-edge region was zero at 6010 eV (Cr) and 7130 eV (Fe) and scaled so that the value of a third order polynomial fit through the region above the edge was unity at these same energies. The Extended X-ray Absorption Fine Structure (EXAFS) were calculated by subtracting the data from a fit of the edge region with the sum of an arctangent and a Gaussian and subsequently approximating the smooth atomic absorption with a polynomial spline function whose knots were adjusted to minimize the area of the Fourier transform modulus of the spectra for R = 0–1.3 Å. These results were then divided by the absorption falloff calculated from the MacMaster coefficients. These knots were checked to ensure they were close to each other for all spectra. The Fourier transforms were calculated on the

Table 1
Composition, additive, and processing atmosphere experimental matrix.

Target hollandite composition	Additive	Atmosphere	Short identifier
$Ba_{1.0}Cs_{0.3}Fe_{2.3}Ti_{5.7}O_{16}$	Ti–TiO_2	Air	Fe–SPH–Ti
		Reduced ($1\%H_2$)	Fe–SPHR–Ti
	n/a	Air	Fe–SPH
		Reduced ($1\%H_2$)	Fe–SPHR
$Ba_{1.0}Cs_{0.3}Cr_{2.3}Ti_{5.7}O_{16}$	Ti–TiO_2	Air	Cr–SPH–Ti
		Reduced ($1\%H_2$)	Cr–SPHR–Ti
	n/a	Air	Cr–SPH
		Reduced ($1\%H_2$)	Cr–SPHR
$Ba_{1.0}Cs_{0.3}Cr_{1.0}Al_{0.3}Fe_{1.0}Ti_{5.7}O_{16}$	Ti–TiO_2	Air	CAF–SPH–Ti
		Reduced ($1\%H_2$)	CAF–SPHR–Ti
	n/a	Air	CAF–SPH
		Reduced ($1\%H_2$)	CAF–SPHR

k^3-weighted spectra after the application of a sine window function to reduce the ripple. For the Cr spectra the range was $k = 2.6–12.0$ Å^{-1} and for Fe the range was $k = 2.8–11.1$ Å^{-1}.

3.3. Cs-incorporation

A crushed sample leaching test was performed in triplicate on each sample to assess Cs-incorporation. Prior to the leaching test, approximately 5 g of each sample were ground in a Tekmar grinder for less than 10 s and the surface area measured using the Brunauer–Emmett–Teller (BET) method for use in later calculations. The mean surface area (for each 5 g sample) was assumed for all sub-samples in a given triplicate set. Also included in the experimental test matrix was the Environmental Assessment (EA) benchmark glass [20], the Approved Reference Material (ARM), the Low-activity Reference Material (LRM), and blanks from the sample cleaning batch. All standards were ground, washed, and prepared according to the standard PCT procedure [21]. Fifteen milliliters of Type-I ASTM water were added to 1.5 g of sample[1] or standard in stainless steel vessels. The vessels were closed, sealed, and placed in an oven at 90 ± 2 °C where the samples were maintained at temperature for 7 days. Once cooled, the resulting solutions were sampled (filtered and acidified), and analyzed. Samples of a multi-element, standard solution were also included as a check on the accuracy of the ICP–AES instrument used for these measurements. Normalized Cs-release was calculated based on the target and measured compositions using the average of the common logarithms of the leachate concentrations according to the equation below,

$$Log[NL_{cs}] = Log\left[\frac{C_{cs}(sample)}{(f_{cs}) \cdot SA/V}\right]$$

where C_{cs} is the concentration of Cs in solution (g/L), f_{cs} is the fraction of Cs in the unleached sample (unitless), SA is the surface area of the sample (m^2), and V is the volume of leachant solution (L) resulting in a normalized Cs release (NL_{cs}) having units of g/m^2. The NL_{cs}s were subsequently normalized to one to compute a unitless figure of merit for Cs-release. This procedure allows for a comparison of Cs incorporation between samples with different compositions, secondary phases and microstructures and is not intended to quantify or predict long term durability of ceramic materials in aqueous environments.

4. Results and discussion

4.1. Processing

All samples were melt processed resulting in sufficient quantities of material with the exception of the Fe–Hol sample with Ti/TiO_2 additions heated in reducing atmosphere (Fe–SPHR–Ti). In general, the Fe–Hol samples exhibited obvious signs of melting and crystallization. The Fe–Hol samples also visibly appeared to have reacted with the alumina crucibles. Indeed, such reactions resulted in the loss of the Fe–SPHR–Ti sample (to the furnace) as previously mentioned. The CAF–Hol samples visibly appeared to have reacted less with the alumina crucible, however several Cr/Al/Fe–Hol samples were not easily removed from the crucible without mechanical means. In general, the CAF–Hol samples exhibited near melting and crystallization as evidenced by visible signs of flowing and adhesion to the crucible. The Cr–Hol samples visibly appeared to have reacted least with the alumina compared to either the Fe–Hol or CAF–Hol samples. The interior of the alumina crucible was pink in color, which is consistent with Cr contamination. In general, the Cr–Hol samples appeared to have reacted (solid-state) but exhibited minimal bulk melting. Instead, these samples were essentially pellets (shaped as the powder consolidated in the crucible) that were easily removed from the crucible by hand.

Although high purity (99.99%) alumina crucibles were considered suitable for the melt processing studies in this work, it is noted that reaction with the alumina crucible was not ideal. However, other refractory crucibles would likely react as well, perhaps to a greater extent depending on the material, and it was not desirable to use precious metal crucibles that alloy under reducing conditions. Furthermore, the effect of alumina impurity on hollandite formation and processing in the studied compositions was not an objective of this research and the results indicate that alumina impurity was not detrimental to the research objectives.

4.2. Chemical composition

The calculated compositions based on measured elemental concentrations and Fe redox measurements for each hollandite are summarized in Table 2. The calculated concentration for each cation was normalized to the expected composition. The oxygen concentration was charge balanced to the calculated cation concentrations and oxidation state. Standard temperature and pressure (STP) oxidation states for Ba, Cs, Al, and Ti were assumed in all samples. For samples synthesized in reducing conditions, all Fe and Cr was assumed to be 2+. For Fe–Hol and CAF–Hol samples synthesized in air, Fe^{2+} and Fe^{3+} concentrations were determined from redox measurements. For Cr–Hol samples synthesized in air, Cr was assumed to be 3+. Adjustments were made to samples to which Ti/TiO_2 was added. (i.e. 2.0 wt.% Ti was subtracted before calculation) Similarly, Al_2O_3 was measured in the Fe–Hol samples, but was not included in the calculated hollandite stoichiometry.

The measured compositions were in good agreement with the target (nominal) compositions with the exception of excess Al_2O_3 in some samples and low Cs concentrations in all samples. The excess alumina in samples was attributed to reactions with the Al_2O_3 crucibles as noted above. In general, the samples processed under reducing conditions exhibited more oxygen deficiency as expected.

The low Cs concentration was attributed to the high volatility of cesium at the processing temperatures and is in agreement with previous work. This work was intended to evaluate melt processing as a suitable method for forming Cs containing hollandite as a crystalline host phase. Although Cs retention after high temperature melt processing was not ideal in all of the measured samples, it is important to note that the low Cs concentrations measured in the as-processed samples does not preclude melt processing as a viable method for several reasons: (i) Cs volatility occurs during other processing routes and the surface to volume ratio of the samples at the laboratory scale enhances volatilization effects compared to what would be expected in a practical process in which much larger volumes would be processed and (ii) typical large scale melt processes employ a cold-cap (not practical in this research) that also enhances volatile species retention. To be sure, further research is needed to understand the high temperature stability of these hollandite compositions.

In samples with Fe, excess Al was measured in increasing concentrations as follows: air → air w/Ti/TiO_2 → 1%H_2 → 1%H_2 w/Ti/TiO_2. The increasing Al concentration with increasing Fe^{2+} concentration indicates the crucible was a source of Al_2O_3 impurity and that the reactions are competing with hollandite formation. This result can be deduced from the FeO–Al_2O_3 phase diagram and is supported by SEM–EDS data presented in the electron microscopy discussion section.

4.3. X-ray diffraction

X-ray diffraction (XRD) confirmed that the samples were, in general, single phase hollandite. All Cr–Hol samples were single phase except the sample heated in air to which Ti/TiO_2 was added, which contained excess rutile (TiO_2). This was not unexpected, as excess TiO_2 was intentionally added and similar results have been reported by other groups. All CAF–Hol samples exhibited a major hollandite phase, but also contained minor titanate phases. In contrast, the Fe–Hol samples, although exhibiting a major hollandite phase, also contained several parasitic phases including titanatates and aluminates. Although these samples were not single phase, the majority of the detected parasitic phases would be expected to be

[1] There was not enough sample to perform the measurement in triplicate for three samples. In those samples, available crushed powder was split into three (or two) equal portions and the water addition was adjusted to maintain the 1:10 ratio of sample to water.

Table 2
Calculated hollandite compositions based on measured elemental concentrations.

Short ID	Nominal composition	ICP composition	Fe^{2+}/Fe^{Tot}
[a]Fe–SPH	$Ba_{1.0}Cs_{0.3}Fe_{2.3}Ti_{5.7}O_{16}$	$Ba_{1.0}Cs_{0.16}Fe_{2.4}Ti_{5.8}O_{15.9}$	0.26
[b,c]Fe–SPH–Ti	$Ba_{1.0}Cs_{0.3}Fe_{2.3}Ti_{5.7}O_{16}$	$Ba_{1.0}Cs_{0.24}Fe_{2.4}Ti_{5.6}O_{15.8}$	0.19
[d]Fe–SPHR	$Ba_{1.0}Cs_{0.3}Fe_{2.3}Ti_{5.7}O_{16}$	$Ba_{1.0}Cs_{0.14}Fe_{2.4}Ti_{5.7}O_{15.0}$	All Fe^{2+}
Cr–SPH	$Ba_{1.0}Cs_{0.3}Cr_{2.3}Ti_{5.7}O_{16}$	$Ba_{1.0}Cs_{0.14}Cr_{2.3}Ti_{5.8}O_{16.2}$	n.m.
[c]Cr-SPH-Ti	$Ba_{1.0}Cs_{0.3}Cr_{2.3}Ti_{5.7}O_{16}$	$Ba_{1.0}Cs_{0.15}Cr_{2.4}Ti_{5.6}O_{16.1}$	n.m.
[e]Cr–SPHR	$Ba_{1.0}Cs_{0.3}Cr_{2.3}Ti_{5.7}O_{16}$	$Ba_{1.0}Cs_{0.19}Cr_{2.3}Ti_{5.8}O_{15.0}$	n.m.
[c,e]Cr–SPHR–Ti	$Ba_{1.0}Cs_{0.3}Cr_{2.3}Ti_{5.7}O_{16}$	$Ba_{1.0}Cs_{0.19}Cr_{2.4}Ti_{5.7}O_{14.9}$	n.m.
CAF–SPH	$Ba_{1.0}Cs_{0.3}Cr_{1.0}Al_{0.3}Fe_{1.0}Ti_{5.7}O_{16}$	$Ba_{1.0}Cs_{0.16}Cr_{1.0}Al_{0.3}Fe_{1.0}Ti_{5.8}O_{16.1}$	0.22
[c]CAF–SPH–Ti	$Ba_{1.0}Cs_{0.3}Cr_{1.0}Al_{0.3}Fe_{1.0}Ti_{5.7}O_{16}$	$Ba_{1.0}Cs_{0.16}Cr_{1.1}Al_{0.4}Fe_{1.0}Ti_{5.7}O_{16.1}$	0.11
[e]CAF–SPHR	$Ba_{1.0}Cs_{0.3}Cr_{1.0}Al_{0.3}Fe_{1.0}Ti_{5.7}O_{16}$	$Ba_{1.0}Cs_{0.15}Cr_{1.0}Al_{0.4}Fe_{1.0}Ti_{5.7}O_{15.6}$	All Fe^{2+}
[c,e]CAF–SPHR–Ti	$Ba_{1.0}Cs_{0.3}Cr_{1.0}Al_{0.3}Fe_{1.0}Ti_{5.7}O_{16}$	$Ba_{1.0}Cs_{0.17}Cr_{0.9}Al_{0.6}Fe_{1.0}Ti_{5.7}O_{15.2}$	All Fe^{2+}

[a] 7 wt.% Al_2O_3 measured.
[b] 10 wt.% Al_2O_3 measured.
[c] ICP compositions adjusted for Ti/TiO_2 addition.
[d] 14 wt.% Al_2O_3 measured.
[e] Adjusted for all Cr^{3+}.

Table 3
Summary of crystalline phases determined from X-ray diffraction XRD measurements and energy dispersive X-ray spectroscopy EDAX elemental analysis.

Short ID	Major phase[a]	Minor phase(s)[b]	Processing conditions
Fe–SPH	Hollandite	$Fe_2Ti_3O_9$; $CsTiAlO_4$	Air
Fe–SPH–Ti	Hollandite	$Fe_3Ti_3O_{10}$; $CsTiAlO_4$	Air w/Ti–TiO_2
Fe–SPHR	Hollandite	$BaFe_{12}O_{19}$; $CsTiAlO_4$; $FeAl_2O_4$	1% H_2
Fe–SPHR–Ti	Hollandite	Al_2O_3; $FeAl_2O_4$	1% H_2 w/Ti–TiO_2
Cr–SPH	Hollandite		Air
Cr–SPH–Ti	Hollandite	TiO_2	Air w/Ti–TiO_2
Cr–SPHR	Hollandite		1% H_2
Cr–SPHR–Ti	Hollandite		1% H_2 w/Ti–TiO_2
CAF–SPH	Hollandite		Air
CAF–SPH–Ti	Hollandite	TiO_2	Air w/Ti–TiO_2
CAF–SPHR	Hollandite	Fe_2TiO_4; $BaFe_{12}O_{19}$; $CsTiAlO_4$	1% H_2
CAF–SPHR–Ti	Hollandite	Fe_2TiO_4	1% H_2 w/Ti–TiO_2

[a] Many hollandite phases exist in the literature. In general, the following PDF files were used to identify the hollandite phases: Fe: 00-051-1900; Cr: 00-039-0352, CAF: 01-076-3178.
[b] The following PDF files were used to identify the minor phases: TiO_2: 00-021-1276; $BaFe_{12}O_{19}$: 00-039-1433; Fe_2TiO_4: 00-034-0177; $FeAl_2O_4$: 01-086-2320; $CsTiAlO_4$: 04-009-3837; $Fe_3Ti_3O_{10}$: 00-047-0421; $Fe_2Ti_3O_9$: 00-0407-1777; Al_2O_3: 00-005-0712.

durable. However, one phase, $CsAlTiO_4$ was also detected and is known to adversely affect Cs retention when subjected to a durability test. The phases identified by XRD are summarized and presented in Table 3.

4.4. Electron microscopy

The microstructure in the Cr–Hol images displayed in Fig. 2 is indicative of a solid state reaction mechanism (with poor densification). The microstructure that is evident in the Fe–Hol sample displayed in Fig. 3 was crystalline with some porosity (relatively large voids) as would be expected from a melt process. Fig. 4 displays the microstructure for the CAF–Hol sample which exhibited a variation between the Cr and Fe analogues where melted areas as well as solid state sintered areas were observed. Although some samples did not appear to have melted at the processing temperature, all samples appeared to have reacted. Hollandite is known to form at much lower temperatures than used in this work and it has been demonstrated that when incorporated into a multiphase waste form, the additional constituents making up the batch will promote melt processing, even of the high refractory Cr containing hollandite samples [22].

Overall, the observed microstructures in Figs. 2 and 4 confirm the XRD results indicating that the Cr–hol samples were single hollandite phase, the CAF–Hol samples exhibited a major hollandite phase accompanied by minor phases, and the Fe–hol samples were multiphase. Semi-quantitative EDS confirmed the composition of many of the various phases. In Figs. 2 and 4 the mid-tone gray color is the major phase and was identified as hollandite. Brighter and darker phases are clearly visible in the figures and are associated with different phases. The brightest phase, which appears generally as white, was rich in Cs and Al and was identified as $CsAlTiO_4$ in most cases. The various darker phases were rich in Fe, Al, and Ti. Excess rutile was identified in Cr- and CAF–Hol samples to which excess Ti/TiO_2 was added. The CAF–Hol samples processed in 1%H_2 (reducing atmosphere) also exhibited secondary Ti-rich phases identified as Fe_2TiO_4 and $FeAl_2O_4$. Rutile was not identified in the Fe–hol samples, instead several Fe- and Al–titanate phases and the $FeAl_2O_4$ compound were identified.

To further understand the reactions occurring during processing and resulting phases and morphology, the CAF–Hol samples were characterized with HRTEM and SEM. Fig. 5, which shows the HRTEM results for the CAF–Hol sample heated in air, indicated the hollandite phase was highly crystalline and contained all the expected elements including Cs. The selected area diffraction pattern shown in the inset of Fig. 5 was indexed to a tetragonal hollandite phase. Elemental maps of the Al, Cs, Fe, and Cr concentrations of Cr/Al/Fe–hol samples heated in 1%H_2 with and without Ti/TiO_2 are presented in Fig. 6. The Cr-rich phase was identified as the pri-

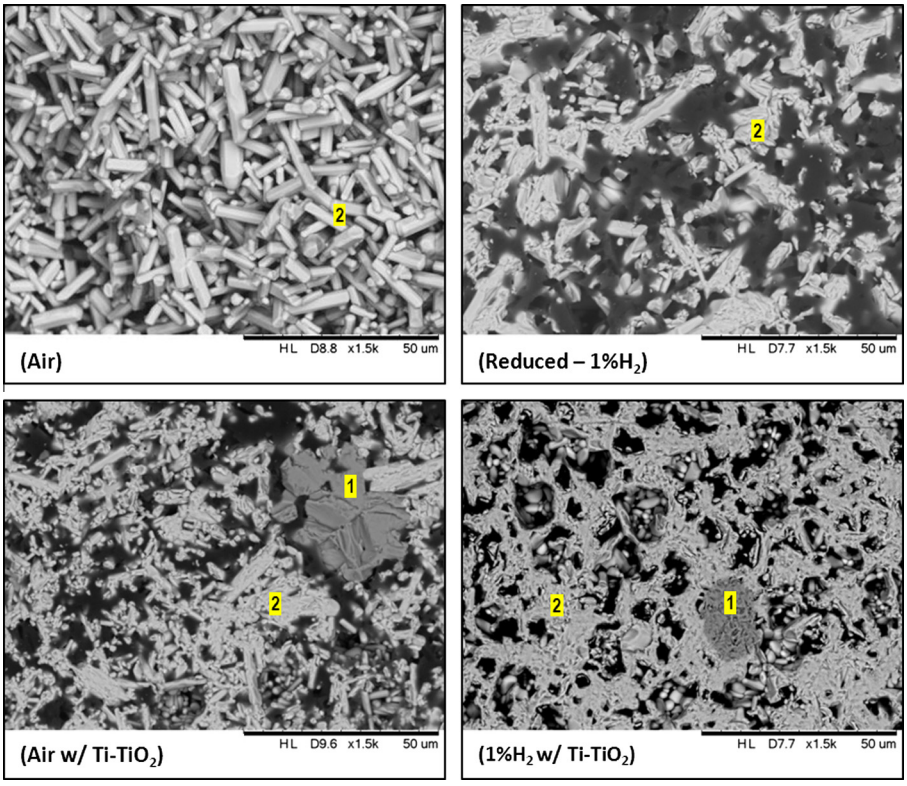

Fig. 2. SEM back scattered detector (BSD) digital images taken of Cr–Hol: $Ba_{1.0}Cs_{0.3}Cr_{2.3}Ti_{5.7}O_{16}$ composition. Labeled phases: (1) rutile and (2) hollandite.

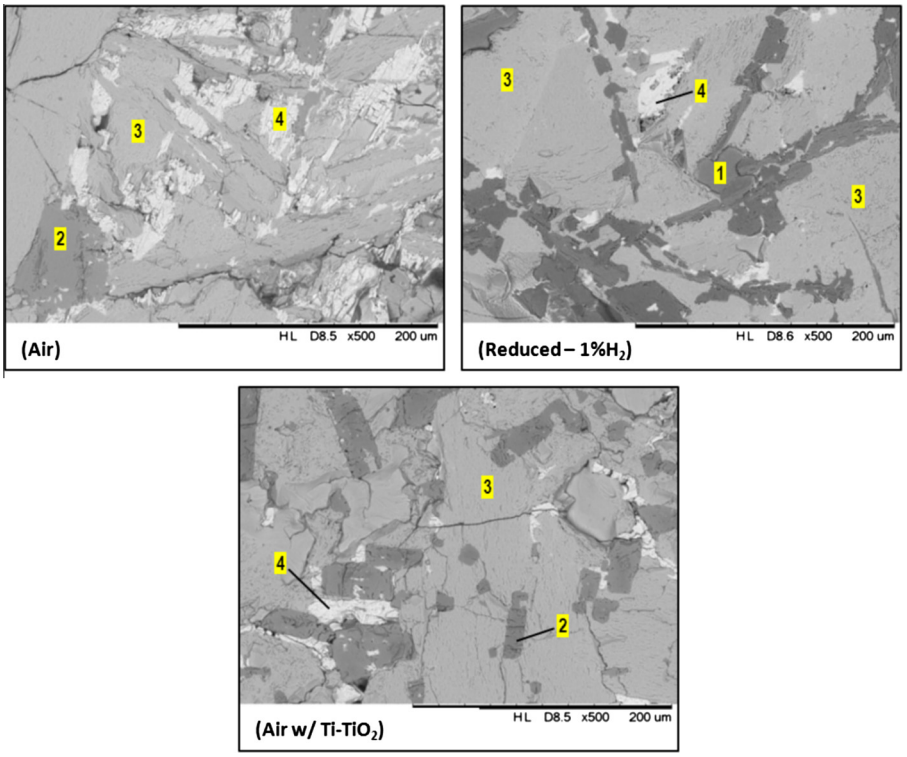

Fig. 3. SEM back scattered detector (BSD) digital images taken of Fe–Hol: $Ba_{1.0}Cs_{0.3}Fe_{2.3}Ti_{5.7}O_{16}$ composition. Labeled phases: (1) $FeAl_2O_4$; (2) ABO_3 ($Fe_3Ti_3O_{10}$); (3) hollandite and (4) $CsAlTiO_4$. Note the Fe–Hol sample heated in 1%H_2 with Ti–TiO_2 was unrecoverable from the furnace.

mary hollandite phase. Fe partitioned mainly to a reduced titanate phase in both samples, but was also distributed along hollandite grain boundaries in the sample processed without Ti/TiO_2 additions. The Cs was associated with the Al in the CAF–Hol sample heated in 1%H_2 without Ti–TiO_2 and is the characteristic bright phase in SEM identified as $CsAlTiO_4$. In contrast, the Cs appeared more distributed in the CAF–Hol sample heated under the same atmosphere, but with Ti/TiO_2 additions.

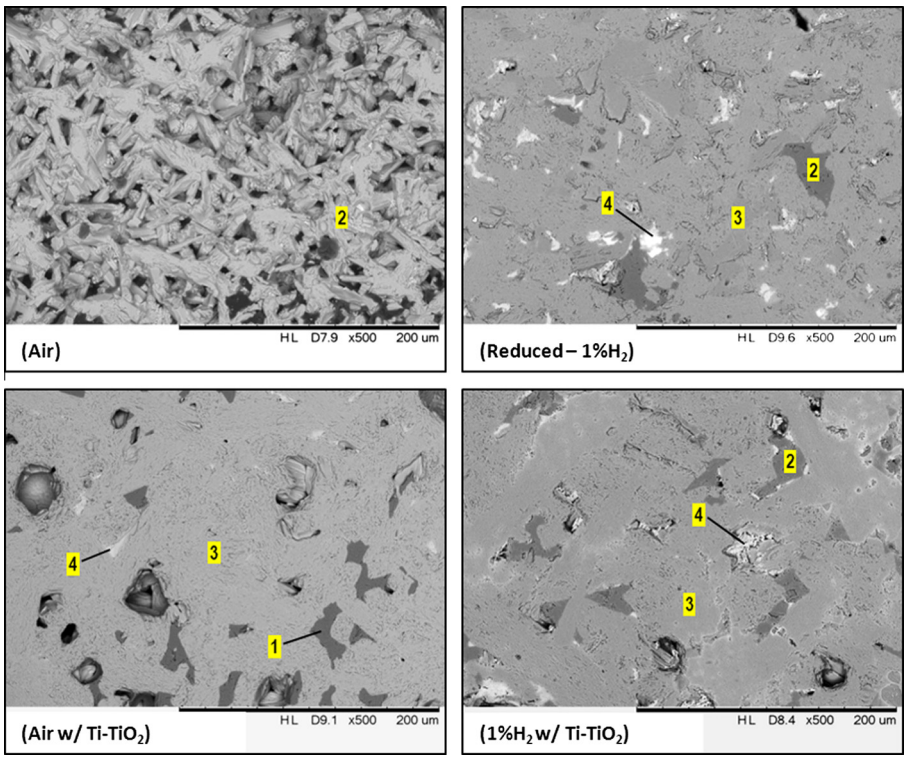

Fig. 4. SEM back scattered detector (BSD) digital images taken of CAF–Hol: $Ba_{1.0}Cs_{0.3}Cr_{1.0}Al_{0.3}Fe_{1.0}Ti_{5.7}O_{16}$ composition. Labeled phases: (1) rutile; (2) Fe_2TiO_4; (3) hollandite and (4) $CsAlTiO_4$.

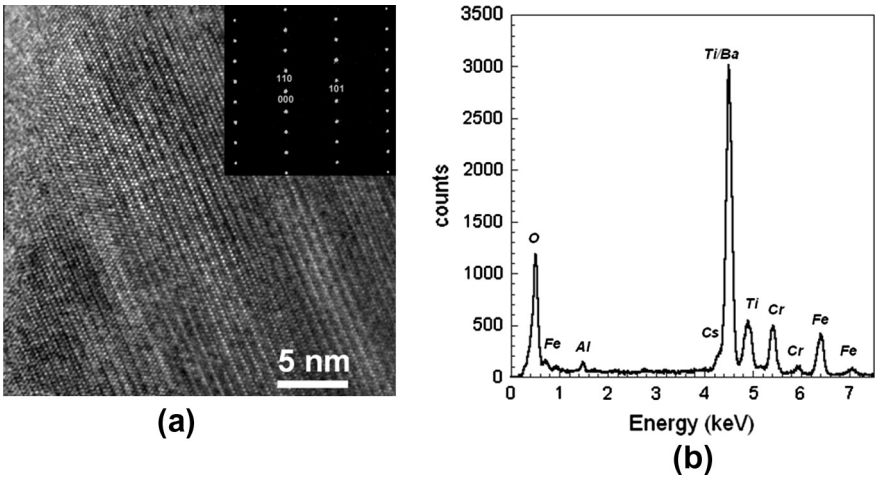

Fig. 5. (a) High resolution transmission electron microscope (HRTEM) image of CAF–SPH melted in air without Ti/TiO_2 (inset SAD indexed to a tetragonal crystal structure) and (b) chemical composition.

The SEM results indicate that reducing agents and processing atmosphere affect hollandite formation and Cs incorporation. Under reducing conditions, melts batched with Fe_2O_3, would be rich in FeO and Al_2O_3 – either from the crucible or from the batch in the case of the CAF–Hol sample – and would precipitate the $FeAl_2O_4$ compound (observed in XRD) which is stable below 1820 °C [23]. The resulting hollandite composition (relative to the starting hollandite) would be deficient in Fe and Al. Indeed, the reduced $FeAl_2O_4$ compound was observed in all Fe-containing samples heated in 1%H_2 whereas the Cr–Hol samples formed a single hollandite phase, under reducing or oxidizing atmospheres. Furthermore, as reduced $FeAl_2O_4$ compounds formed, the hollandite composition was driven off-stoichiometry, which in turn promoted several intermediate $FeO–Fe_2O_3–TiO_2$ compounds known to exist in equilibrium at or below the processing temperatures used in this research [24,25]. This effect was strongest in the Fe–Hol samples processed in reducing conditions without Ti/TiO_2 in which the high concentration of Fe combined with the low melting temperature increased the driving force for high-temperature secondary phase formation.

Although these effects appeared to be compounding in the case of Fe additions (i.e. secondary phases were formed at the expense of hollandite), the addition of Cr and Ti/TiO_2 buffer appear to stabilize the hollandite structure and increase Cs incorporation. The use of Ti/TiO_2 to promote Cs retention has been reported by several authors and has been attributed to the replacement of Al^{3+} by

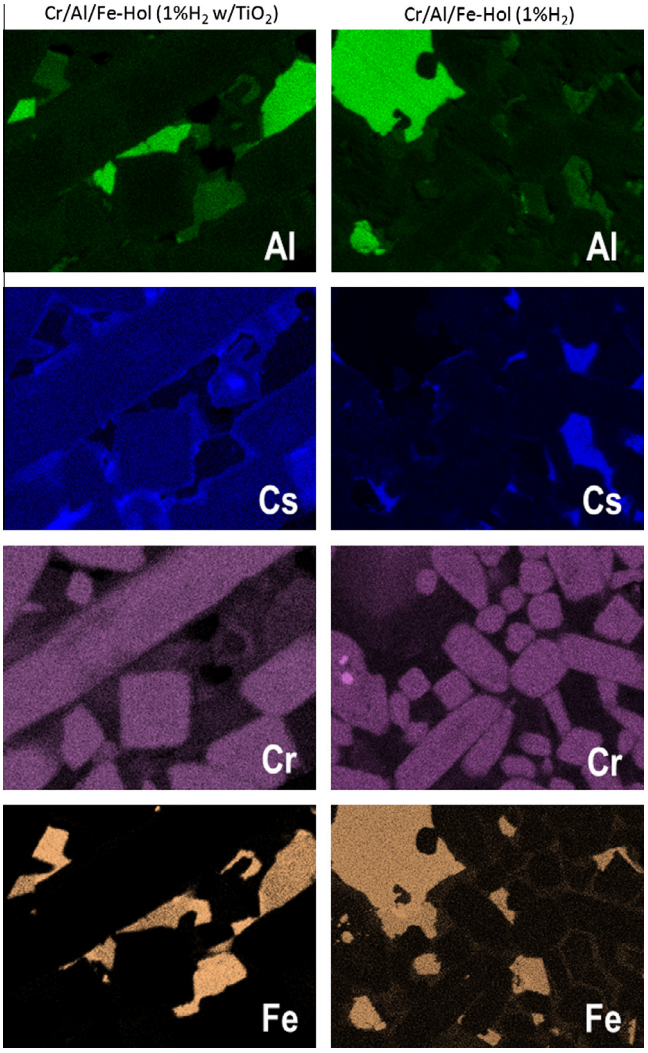

Fig. 6. Select SEM–EDS elemental maps for CAF–Hol: $Ba_{1.0}Cs_{0.3}Cr_{1.0}Al_{0.3}Fe_{1.0}Ti_{5.7}O_{16}$ compositions heated in various atmosphere.

Ti^{3+} without consuming hollandite. Indeed, the SEM results in this work indicate that Ti/TiO_2 added to samples processed in air inhibits the parasitic $CsAlTiO_4$ phase formation compared to samples heated in $1\%H_2$ without Ti/TiO_2. The role of Cr is less understood and has not been studied in detail to date. This research suggests that Cr preferentially enters the hollandite phase (even in the presence of competing phases). Due to its refractory nature, Cr does not form compounds readily with Cs and Cr^{3+} is not easily susceptible to reduction. Cr_2O_3 appears to stabilize the hollandite phase which in turn should promote Cs incorporation. This is visually observed in the SEM images by comparing the relative area of bright phase ($CsAlTiO_4$) across all samples and within each composition group.

4.5. X-ray absorption spectroscopy

X-ray absorption near edge spectroscopy (XANES) was used to confirm the average oxidation states of the Fe and the Cr in the CAF–Hol samples. Normalized XANES spectra are shown for Fe and Cr in Fig. 7. XANES was used to identify changes in the average oxidation states of the Fe and the Cr resulting from the changes in composition and processing conditions. The Cr XANES and $\chi(R)$ EXAFS are identical within the experimental uncertainty, showing that Cr speciation is unaffected by the processing. The spectra are clearly those of Cr(III), not exhibiting the intense pre-edge peak characteristic of Cr(VI) that originates in the non-centrosymmetric environment of these species. Insofar as the original speciation is Cr(III) it is not surprising that processing under H_2 has no effect. The EXAFS display a high degree of order extending out through the fourth or fifth near neighbor shell. The Fe XANES clearly show a change in the samples processed with H_2. The shift of the absorption edge to lower energy is consistent with the reduced species that would be expected to form under these conditions, with the extent of the shift within the range for the reduction of Fe(III) to (II). This change in speciation is also obvious in the EXAFS. The nearest neighbor peaks that represent the O shell are not only lower in amplitude but also shifted to higher R, with the second near neighbor peaks showing an even greater expansion in distance. The addition of the Ti appears to have minimal or negligible effects on the Fe speciation.

5. Durability

A standardized durability measurement has yet to be developed for alternative ceramic waste forms. Nevertheless, several different studies of hollandite durability have reported a relatively quick initial loss of Cs. This behavior has been attributed to soluble Cs containing impurity phases ($CsAlTiO_4$ and Cs_2MoO_4) and intergranular films enriched with Cs formed during processing [8,26]. Leaching tests were performed in this research to assess the comparative Cs incorporation and stability within the ceramic between the three hollandite compositions synthesized under the various processing conditions. The leaching test was intended to provide a

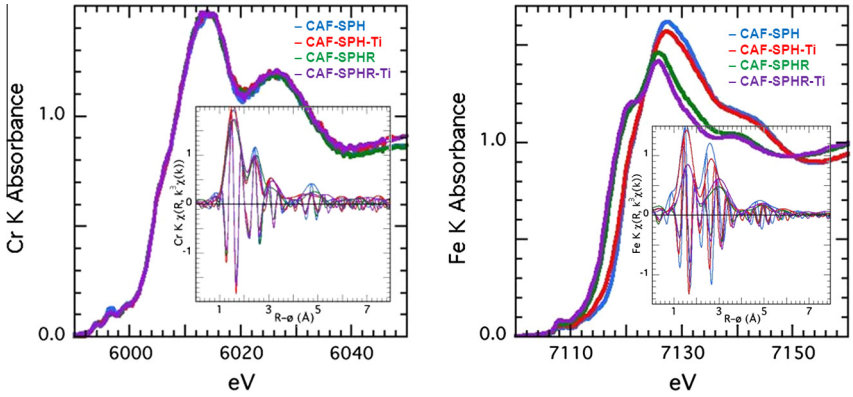

Fig. 7. (a) Cr and (b) Fe XANES and EXAFS spectra of CAF–Hol: $Ba_{1.0}Cs_{0.3}Cr_{1.0}Al_{0.3}Fe_{1.0}Ti_{5.7}O_{16}$ processed in air (SPH); processed in air with Ti/TiO_2 (SPH-Ti); processed in $1\%H_2$ (SPHR); processed in $1\%H_2$ with Ti/TiO_2 (SPHR-Ti), according to the guide. The insets show the moduli and real components of the EXAFS in the (R) representation.

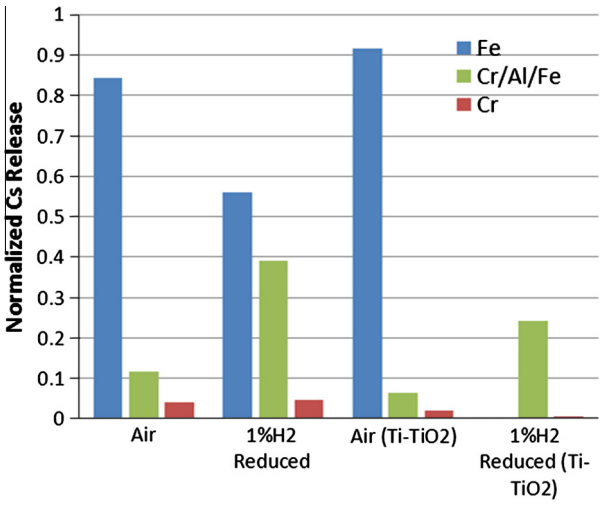

Fig. 8. Normalized Cs release for Fe–Hol: $Ba_{1.0}Cs_{0.3}Fe_{2.3}Ti_{5.7}O_{16}$ (Fe), CAF–Hol: $Ba_{1.0}Cs_{0.3}Cr_{1.0}Al_{0.3}Fe_{1.0}Ti_{5.7}O_{16}$ (CAF), and, Cr–Hol: $Ba_{1.0}Cs_{0.3}Cr_{2.3}Ti_{5.7}O_{16}$ (Cr).

qualitative measure of the Cs incorporation into the various hollandite compositions based on the assumption that parasitic Cs-rich phases control the initial Cs loss in leach tests. The measured Cs release was normalized to the measured surface area (0.1–0.4 m^2/g) for each sample. The Cs release across the samples for a given processing route was then normalized to one. The normalized Cs release summarized in Fig. 8, indicated that the Fe–Hol sample exhibited the least Cs retention whereas the Cr–Hol sample exhibited the greatest Cs retention. The comparative Cs retention is supported by XRD and SEM analysis in which the Cr sample was found to be phase pure (excepting excess rutile) whereas the CAF–Hol and Fe–Hol samples exhibited secondary phases enriched in Cs. The addition of Ti/TiO_2 appeared to increase the Cs retention in the Cr and CAF samples (to clarify, the increase was measured for the same processing atmosphere, not across air and $1\%H_2$). The Cs retention was greater in samples not heated under reducing conditions. This result can be explained by the characterization results, which indicated reducing environments favor secondary phase formation that compete for Cs retention with the hollandite. Luca et al. has suggested a Ti^{3+} oxidation reaction (to promote Cs extraction at the surface) mechanism for Cs release in a reduced hollandite ($Cs_{0.8}Ba_{0.4}Ti_8O_{16}$) which has been supported by Angeli et al. that reported Cs leaching from a mixed trivalent hollandite ($BaCs_{0.28}Fe_{0.82}Al_{1.46}Ti_{5.72}O_{16}$) [26,27]. Although this study does not directly support such a mechanism, this study appears to indicate that Cr is useful in stabilizing the hollandite phase in two ways; (i) it promotes hollandite formation providing a phase for Cs incorporation and (ii) the hollandite phase is more stable as the Cr is not readily reduced or easily substituted for other trivalent cations.

6. Conclusions

This work details the impact of Cr additions on Cs containing hollandites of the form $Ba_{1.0}Cs_{0.3}A_{2.3}Ti_{5.7}O_{16}$; A = Cr, Fe, Al. Relative durability studies indicated that the Fe–Hol sample exhibited the least Cs retention whereas the Cr–Hol sample exhibited the greatest Cs retention. The comparative Cs retention is supported by XRD and SEM analysis indicating that the CAF–Hol and Fe–Hol samples exhibited secondary phases enriched in Cs; the presence of these phases were enhanced under reducing processing conditions. Secondary phase formation under reducing conditions was inhibited by Cr additions due to the stability of the Cr^{+3} as compared to Fe^{+3} as measured by X-ray absorption spectroscopy. Hollandite compositions with Cr additions are considered a promising Cs-containing phase to be used in melt processing of multi-phase waste forms for advanced nuclear fuel cycles.

Acknowledgements

This document was prepared in conjunction with work accomplished under Contract No. DE-AC09-08SR22470 with the U.S. Department of Energy. The authors acknowledge gratefully the financial support of the DOE-NE Separations and Waste Form program including program support from John Vienna and Terry Todd. D. Missimer gratefully acknowledged for processing and characterization work.

References

[1] J.V. Crum, L. Turo, B. Riley, M. Tang, A. Kossoy, Multi-phase glass–ceramics as a waste form for combined fission products: alkalis, alkaline earths, lanthanides, and transition metals, J. Am. Ceram. Soc. 95 (2012) 1297–1303.
[2] J.D. Vienna, Nuclear waste vitrification in the united states: recent developments and future options, Int. J. Appl. Glass Sci. 1 (2010) 309–321.
[3] A.L. Billings, K. Brinkman, K. Fox, J.C. Marra, M. Tang, Preliminary Study of Ceramics for Immobilization of Advanced Fuel Cycle Reprocessing Wastes, FCRD-WAST-2010-000158, 2010.
[4] K. Brinkman, K. Fox, J. Marra, M. Tang, Crystalline Ceramic Waste Forms: Reference Formulation Report, Savannah River National Laboratory Technical Report: SRNL-STI-2012-00281, FCRD-SWF-2012-000116, 2012.
[5] K. Brinkman, K. Fox, M. Tang, Development of Crystalline Ceramics for Immobilization of Advanced Fuel Cycle Reprocessing Wastes, Savannah River National Laboratory Technical Report: SRNL-STI-2011-00516, FCRD-SWF-2011-000310, 2011.
[6] A.E. Ringwood, S.E. Kesson, N.G. Ware, W. Hibberson, A. Major, Immobilization of high-level nuclear reactor wastes in SYNROC, Nature 278 (1979) 219–223.
[7] A.E. Ringwood, S.E. Kesson, N.G. Ware, W.O. Hibberson, A. Major, SYNROC process – geochemical approace to nuclear waste immobilization, Geochem. J. 13 (1979) 141–165.
[8] S.E. Kesson, The immobilization of cesium in SYNROC hollandite, Radioact. Waste Manage. Environ. Restor. 4 (1983) 53–72.
[9] H.F. Xu, Y.F. Wang, Crystallization sequence and microstructure evolution of SYNROC samples crystallized from $CaZrTi_2O_7$ melts, J. Nucl. Mater. 279 (2000) 100–106.
[10] S.V. Stefanovsky, A.G. Ptashkin, O.A. Knyazev, S.A. Dmitriev, S.V. Yudintsev, B.S. Nikonov, Inductive cold crucible melting of actinide-bearing murataite-based ceramics, J. Alloy. Comp. 444 (2007) 438–442.
[11] C. Biagioni, P. Orlandi, M. Pasero, Ankangite from the monte arsiccio mine (Apuan Alps, Tuscany, Italy): occurrence, crystal structure, and classification problems in cryptomelane group minerals, Period. Mineral. 78 (2009) 3–11.
[12] R.W. Cheary, J. Kwiatkowska, An X-ray structural-analysis of cesium substitution in the barium hollandite phase of SYNROC, J. Nucl. Mater. 125 (1984) 236–243.
[13] M.L. Carter, E.R. Vance, D.R.G. Mitchell, J.V. Hanna, Z. Zhang, E. Loi, Fabrication, characterization, and leach testing of hollandite, (Ba, Cs)(Al, Ti)$2Ti_6O_{16}$, J. Mater. Res. 17 (2002) 2578–2589.
[14] V. Aubin-Chevaldonnet, D. Caurant, A. Dannoux, D. Gourier, T. Charpentier, L. Mazerolles, T. Advocat, Preparation and characterization of (Ba, Cs)$(M, Ti)_8 O_{16}$ ($M = Al^{3+}$, Fe^{3+}, Ga^{3+}, Cr^{3+}, Sc^{3+}, Mg^{2+}) hollandite ceramics developed for radioactive cesium immmobilization, J. Nucl. Mater. 366 (2007) 137–160.
[15] M.L. Carter, E.R. Vance, H. Li, Hollandite-rich ceramic melts for immobilization of Cs, Mater. Res. Soc. Symp. Proc. 807 (2004) 1–6.
[16] M.L. Carter, E.R. Vance, D.R.G. Mitchell, Z. Zhang, Mn oxidation states in $Ba_xCs_yMn_zTi_{8-z}O_{16}$, Mater. Res. Soc. Symp. Proc. 824 (2004) CC4.6.1.
[17] W.J. Buykx, K. Hawkins, D.M. Levins, H. Mitamura, R.S. Smart, G.T. Stevens, K.G. Watson, D. Weedon, T.J. White, Titanate ceramics for the immobilization of sodium-bearing high-level nuclear waste, J. Am. Ceram. Soc. 71 (1988) 678–688.
[18] H.S. Potdar, S. Vijayanand, K.K. Mohaideen, K.R. Patil, P.A. Joy, R.R. Madhavan, K.V.G. Kutty, R.D. Ambashta, P.K. Wattal, A simple chemical co-precipitation/calcination route for the synthesis of simulated SYNROC-B and SYNROC-C powders, Mater. Chem. Phys. 123 (2010) 695–699.
[19] E.W. Baumann, Colorimetric Determination of Ferrous-Ferric Ratio in Glass, US Department of Energy Report DPST-87-304, Savannah River Laboratory, Aiken, 1987.
[20] C.M. Jantzen, N.E. Bibler, D.C. Beam, C.L. Crawford, M.A. Pickett, Characterization of the Defense Waste Processing Facility (DWPF) Environmental Assessment (EA) Glass Standard Reference Material. U.S. Department of Energy Report WSRC-TR-92-346 Rev. 1, Westinghouse Savannah River Company, Aiken, SC, 1993.
[21] Standard Test Methods for Determining Chemical Durability of Nuclear, Hazardous, and Mixed Waste Glasses and Multiphase Glass Ceramics: The Product Consistency Test (PCT), ASTM C-1285-02, 2002.

[22] K. Brinkman, J. Amoroso, J. Marra, M. Tang, Crystalline Ceramic Waste Forms: Comparison of Reference Process for Ceramic Waste Form Fabrication, SRNL Technical Report- FCRD-SWF-2013-000229, 2013.
[23] K. Rosenbach, J.A. Schmitz, A. Eisenhuettenwes. Retrieved from ACerS-NIST Phase Equilibrium Diagrams, CD-ROM Database, Version 3.3.0, Figure 05152, vol. 45 (12) (1974) pp. 843–47.
[24] J.B. MacChesney, A. Muan, Am. Mineral 44 (9-10) (1959) 926–945. Retrieved from ACerS-NIST Phase Equilibrium Diagrams, CD-ROM Database, Version 3.3.0, Figure 00090.
[25] R.W. Taylor, J. Am. Ceram. Soc. 46 (6) (1963) 276–279. Retrieved from ACerS-NIST Phase Equilibrium Diagrams, CD-ROM Database, Version 3.3.0, Figure 02170.
[26] F. Angeli, P. McGlinn, P. Frugier, Chemical durability of hollandite ceramic for conditioning cesium, J. Nucl. Mater. 380 (2008) 59–69.
[27] V. Luca, D. Cassidy, E. Drabarek, K. Murray, B. Moubaraki, Cesium extraction from $Cs_{0.8}Ba_{0.4}Ti_8O_{16}$ hollandite nuclear waste form ceramics in nitric acid solutions, J. Mater. Res. 20 (2005) 1436–1446.